Tao Liang[a], Zheng Chen[a], Xiaoqin Yang[b], Jinyong Zhang[a], Ping Zhang[a]
[a] School of Material Science and Engineering, China University of Mining and Technology, Xuzhou, P.R. China
[b] School of Chemical Engineering and Technology, China University of Mining and Technology, Xuzhou, P.R. China

The thermodynamic stability induced by solute co-segregation in nanocrystalline ternary alloys

The grain growth and thermodynamic stability induced by solute co-segregation in ternary alloys are presented. Grain growth behavior of the single-phase supersaturated grains prepared in Ni–Fe–Pb alloy melt at different undercoolings was investigated by performing isothermal annealings at $T = 400\,^{\circ}\mathrm{C} - 800\,^{\circ}\mathrm{C}$. Combining the multicomponent Gibbs adsorption equation and Guttmann's grain boundary segregation model, an empirical relation for isothermal grain growth was derived. By application of the model to grain growth in Ni–Fe–Pb, Fe–Cr–Zr and Fe–Ni–Zr alloys, it was predicted that driving grain boundary energy to zero is possible in alloys due to the co-segregation induced by the interactive effect between the solutes Fe/Pb, Zr/Ni and Zr/Cr. A non-linear relationship rather than a simple linear relation between $1/D^*$ (D^* the metastable equilibrium grain size) and $\ln(T)$ was predicted due to the interactive effect.

Keywords: Thermodynamic stability; Co-segregation; Ternary alloy; Grain growth

1. Introduction

Nanocrystalline (NC) materials (grain size <100 nm) have unique properties compared with their coarse grained counterparts [1, 2]. However, thermally driven grain-size instability limits the processing and applications of NC metals. It has been observed that some alloys retain a nano-scale grain size at high temperatures through solute segregation, which can be attributed to kinetic or thermodynamic stabilization effects. Kinetic stabilization of grain size slows the rate at which grain growth progresses [3, 4]. Thermodynamic stabilization reduces the grain boundary (GB) energy [1]. Weissmüller [5], Krill [6] and Kirchheim et al. [7] investigated thermodynamic stabilization for binary alloys using the Gibbs adsorption equation. Subsequently, the study of thermodynamic stabilization was further extended to concentrated alloys by Trelewicz and Schuh [8].

All the above models and experiments were based on the effect of single solute on stabilization of NC alloys (i.e., binary alloys). This seriously limited the development of new NC alloys with high stabilization. In 1975, Guttmann [9] developed a model for GB segregation in non-ideal multicomponent systems and worked out an analytical solution for simple ternary alloys. If two elements strongly attract one another, they will precipitate in the matrix. However, if their interaction is less strongly attracted they will co-segregate to the boundaries to lower the free energy of the system. Furthermore, the segregation of one element can induce segregation of the other one. This model could explain why the addition of alloys enhanced impurity segregation [9, 10]. Stabilization of nano-scale grain size in base binary alloys by adding suitable ternary or multi solutes has been reported in recent investigations [11]. The effect of zirconium addition on grain size stability of mechanically alloyed NC Fe–Cr or Fe–Ni alloy was reported by Saber et al. [12, 13]. Zr and Y were also used as an addition to NC Cu–Al alloy to improve its stabilization and strength at high temperatures [11]. The doping of La^{3+} and Y^{3+} into zirconia (YSZ) was designed to obtain stabilized YSZ by targeting a decrease in average GB energy [14]. However, in these investigations, the share of each solute in thermodynamic stabilization and the interactive effect of solutes (i.e., solute co-segregation) on the grain growth have not been distinguished theoretically.

This work aims to present a simple analytical model describing thermodynamic stabilization of nano-scale grain size in multi-component alloys. Then the model will be applied to the grain growth process of Ni–Fe–Pb, Fe–Ni–Zr and Fe–Cr–Zr alloys and the contribution of each solute–solute and solute–solvent interaction parameters will be elucidated.

2. Experimental procedure

Using glass fluxing combined with cyclic superheating and rapid quenching into a Ga–In–Sn bath after recalescence, a homogeneous supersaturated grain was obtained for undercooled Ni–Fe–Pb alloy melts with 1.5 at.% Fe and 1 at.% Pb. The detailed experimental procedure is available in Ref. [15].

To investigate the behavior of grain growth and solute segregation, isothermal anneals at different temperatures ($400 - 800\,^{\circ}\mathrm{C}$) were conducted in a vacuum electrical-resistance furnace under the protection of an argon atmosphere. The as-solidified and as-annealed samples of the undercooled Ni–Fe–Pb alloy were sectioned, polished and etched

by using 5 g $FeCl_3$ + 10 mL HCl + 100 mL H_2O. The microstructure of as-annealed samples was obtained by using an OLYMPUS–PMG3 optical microscope. The grain size was measured by using a Leco image analysis instrument. The structures of GB and precipitated phases and their corresponding selected-area electron diffraction (SAED) patterns were analyzed by transmission electron microscopy (TEM, JEM 2100 microscope). The concentration distribution was detected by TEM-EDS (energy-dispersive X-ray spectroscopy).

3. Model derivation

The basic assumptions are known that the fixed number of the adsorbing site for free surface adsorption corresponds simply to the sites equivalent of a completed monatomic layer of adsorbate. Guttmann developed a series of theories to allow for interactions between two co-segregation species in ternary or higher order systems [9],

$$\frac{X_{bi}}{C_{bi0}} = \frac{x_{ci}\exp(-\Delta G_i/RT)}{1+\sum_{j=1}^{2} x_{cj}\left[\exp\left(\frac{\Delta G_j}{RT}\right)-1\right]} \tag{1}$$

where X_{bi0} is the fraction of the GB monolayer available for segregated atoms at saturation, X_{bi} is the actual fraction, X_{b1} and X_{b2} are typically the molar fractional monolayers segregated by the impurity and alloying elements of bulk contents X_{c1} and X_{c2}, respectively, as for a ternary dilute system. Additionally,

$$\Delta G_1 = \Delta G_1^0 + \alpha'_{12} X_{b2} \tag{2}$$

$$\Delta G_2 = \Delta G_2^0 + \alpha'_{12} X_{b1} \tag{3}$$

where ΔG_1^0 and ΔG_2^0 are the free energies of segregation of the impurity and alloying elements separately in the matrix. The interaction coefficients α'_{12} refer to the changes in nearest-neighbor bond energies in forming the alloy-impurity bonds. The numerical values have been determined from the heat of mixing but better values can be obtained from measurements of the effects of the alloy elements on the solubility of the impurities. In the first approach, with some simplifications [9],

$$\alpha'_{12} = \alpha_{12} - \alpha_{23} - \alpha_{13} \tag{4}$$

where the subscripts 1, 2 and 3 refer to the impurity, alloy and matrix atoms, respectively. The α_{ij} are in turn the binary molar regular solution parameters defined by [10],

$$\alpha_{ij} = ZN_0\left[\varepsilon_{ij} - \frac{(\varepsilon_{ij}+\varepsilon_{ij})}{2}\right] \tag{5}$$

where Z is the coordination number and N_0 is Avogadro's number. The ε_{ij} is simply the interaction energy between the nearest-neighbour atoms i and j.

The most general form of Gibbs adsorption theorem can be expressed by [16],

$$\mathrm{d}\sigma = -S\mathrm{d}T - \sum_i \Gamma_i \mathrm{d}\mu_i \tag{6}$$

with σ as the GB energy analogous to the surface tension, S the entropy, Γ_i and μ_i the density of the ith component at the GB and its chemical potential, respectively. The dilute homogeneous binary alloys at constant temperature are, certainly, the most relevant and interesting from the GB segregation point of view. Using the Gibbs–Duhem equation and Henry's law, Eq. (6) reduces to,

$$\mathrm{d}\sigma = -\left(\frac{\Gamma_2^1 RT\mathrm{d}X_2}{X_2} + \frac{\Gamma_3^1 RT\mathrm{d}X_3}{X_3}\right) \tag{7}$$

where 1 is considered as a solvent and elements 2 and 3 as weakly attracted solutes. Γ_2^1 and Γ_3^1 are the solute excess at GBs, which can be expressed as $X_{b2}\Delta\rho$ and $X_{b3}\Delta\rho$, with ρ and Δ as the density and thickness (about 0.8 nm [17]) of the GB, respectively. Assuming that X_3 is constant, Eq. (7) can be simplified as,

$$\mathrm{d}\sigma = -\frac{\Gamma_2^1 RT\mathrm{d}X_2}{X_2} \tag{8}$$

From Eq. (1),

$$X_{b2} = \frac{X_{b20}C_2\exp\left(\frac{\Delta G_2}{RT}\right)}{1-X+X_2\exp\left(\frac{\Delta G_2}{RT}\right)-X_3+X_3\exp\left(\frac{\Delta G_3}{RT}\right)} \tag{9}$$

Given the boundary conditions: $X = 0$, $\sigma = \sigma_b$ for pure solvent; $X = X_2$, $\sigma = \sigma_b$ for binary alloy, integration of Eqs. (8) and (9) gives,

$$\int_{\sigma_0}^{\sigma_b} \sigma = -\Delta\rho RTX_{b0} \int_0^{X_2} \frac{\exp\left(\frac{\Delta G_2}{RT}\right)}{1-X_2+X_2\exp\left(\frac{\Delta G_2}{RT}\right)-X_3+X_3\exp\left(\frac{\Delta G_3}{RT}\right)}\mathrm{d}X_2 \tag{10}$$

And then,

$$\sigma_b - \sigma_0 = -\Delta\rho RTX_{b0}\frac{\exp\left(\frac{\Delta G_2}{RT}\right)}{\exp\left(\frac{\Delta G_2}{RT}\right)-1}\ln\left[\left(1+X_3\exp\left(\frac{\Delta G_3}{RT}\right)\right) -X_3+\exp\left(\frac{\Delta G_2}{RT}\right)-1\right)X_2] + \Delta\rho RTX_{b0}\frac{\exp\left(\frac{\Delta G_2}{RT}\right)}{\exp\left(\frac{\Delta G_2}{RT}\right)-1} \ln\left[\left(1+X_3\exp\left(\frac{\Delta G_3}{RT}\right)-X_3\right)\right] \tag{11}$$

By assuming $\Delta G_2 \gg RT$, $\Delta G_3 \gg RT$ [18], Eq. (11) can be further given as,

$$\sigma_b = \sigma_0 - RT\Gamma_{20}\ln\left[X_3\exp\left(\frac{\Delta G_3}{RT}\right)+X_2\exp\left(\frac{\Delta G_2}{RT}\right)\right] + RT\Gamma_{20}\ln X_3 + \Gamma_{20}\Delta G_3 \tag{12}$$

Similarly, assuming that X_2 is constant, we can also get,

$$\sigma_b = \sigma_0 - RT\Gamma_{30}\ln\left[X_2\exp\left(\frac{\Delta G_2}{RT}\right)+X_3\exp\left(\frac{\Delta G_3}{RT}\right)\right] + RT\Gamma_{30}\ln X_2 + \Gamma_{30}\Delta G_2 \tag{13}$$

Considering the interactive effect of solutes in multicomponent, an integrated equation of GB energy can be obtained,

$$\sigma_b = \sigma_0 - RT\left(\frac{\Gamma_{20}+\Gamma_{30}}{2}\right)\ln\left[\left(x_{30}-\frac{3\Gamma_{b3}V_m}{D*}\right)\exp\left(\frac{\Delta G_3}{RT}\right)+\left(x_{20}-\frac{3\Gamma_{b2}V_m}{D*}\right)\exp\left(\frac{\Delta G_2}{RT}\right)\right] + \frac{1}{2}\left[RT\Gamma_{20}\ln\left((x_{30}-\frac{3\Gamma_{b3}V_m}{D*}\right)+RT\Gamma_{30}\ln\left((x_{20}-\frac{3\Gamma_{b2}V_m}{D*}\right)+\Gamma_{20}\Delta G_3+\Gamma_{30}\Delta G_2\right] \quad (14)$$

In addition, Eq. (14) can be developed to multicomponent alloys as,

$$\sigma_b = \sigma_0 - RT\frac{\sum_{i=2}^{i=n}\Gamma_{i0}}{n-1}\ln\left[\sum_{i=2}^{i=n}\left(x_{i0}-\frac{3\Gamma_{bi}V_m}{D^*}\right)\exp\left(\frac{\Delta G_3}{RT}\right)\right]+\frac{1}{n-1}\sum_{i=2}^{i=n}\sum_{j=2}^{j=n}[RT\Gamma_{i0}\ln\left(x_{j0}-\frac{3\Gamma_{bj}V_m}{D^*}\right)+\Gamma_{i0}\Delta G_j\Big] \quad (i\neq j) \quad (15)$$

The last term of Eqs. (14) and (15) is the change of grain growth driving force caused by the solutes atoms interaction. In Eq. (15), when $n = 2$, namely for the binary alloy, the last term was eliminated, and we can get the same equation as Liu et al. [18]. Hence there exists a state at which the polycrystal is stable with respect to the variation of solute or stable phase at GBs and grain growth leads to a more stable equilibrium when compared with an unchanged grain size and solute segregation. A metastable thermodynamic equilibrium (metastable grain size D^*) is then obtained when σ_b is equal to "0" according to Eq. (14).

4. Experimental results, model application and discussion

4.1. Grain growth and solute co-segregation in Ni–Fe–Pb alloy at different undercoolings

4.1.1. Formation of single-phase supersaturated grains

The as-solidified microstructure of the single-phase supersaturated grain (with $\Delta T = 200$, 220, 230 K) is shown in Fig. 1. Using TEM-EDS the composition of the alloy was determined to be about 97.5 at.% Ni, 1.5 at.% Fe and 1 at.% Pb, with no detectable contamination. From the analysis of EDS, the solute distribution in a single grain was almost uniform, indicating that the solute segregation was suppressed through the rapid solidification and solute trapping effect of undercooled melt. The microstructural evolution and the refinement mechanism of the highly-undercooled rapid solidification in Ni-based alloys have been studied extensively. An important outcome of high undercooling experiments is the observation of an abrupt grain refinement at a critical value ΔT^* which has been analyzed in a variety of Ni-based alloys, such as pure Ni [19], Ni–B [15], DD3 [19], Ni–Cu [20] and Ni–C [21]. It indicates that

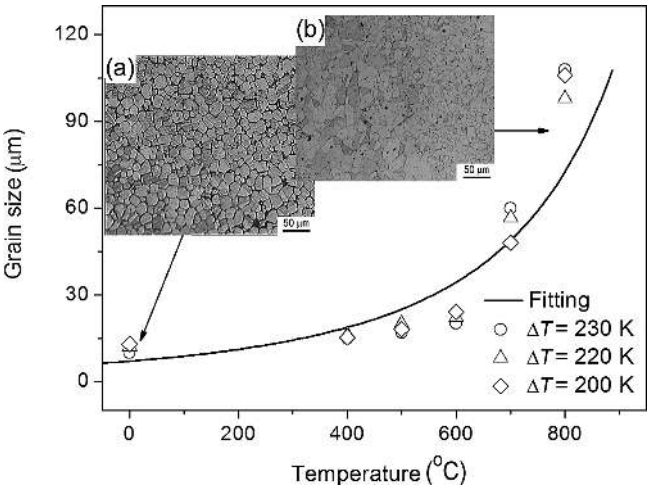

Fig. 1. Fit using Eq. (12) to the evolution of the grain size obtained in Ni-1.5 at.% Fe-1 at.% Pb alloy with temperature. (a) The as-solidified grain at $\Delta T = 220$ K; (b) The as-annealed grain at 800 °C.

the grain refinement transition is a rather universal process occurring in undercooled melts. However, the as-formed single-phase equiaxed grains were not the final stabilized microstructure [22]. On this basis, the grain growth process of the grains in undercooled Ni-1.5 at.% Fe-1 at.% Pb alloy will be clarified.

4.1.2. Heat treatment of the as-solidified grains

The grain size established from OM and TEM is plotted in Fig. 1. Obvious grain growth occurred with the annealing time and annealing temperatures. Figure 2 shows the bright-field TEM images of undercooled Ni–Fe–Pb alloy at $\Delta T = 220$ K at different annealing temperatures. In all samples GBs tended to become thicker with the annealing time increasing, and finally precipitated particles formed, as shown in Fig. 2c. It could be attributed to the segregation of significant solutes (Fe or Pb). The SAED pattern of the sample annealed at 800 °C for 60 min is plotted in Fig. 2d and e, where only α-Ni phase is evidenced in the grain inner and $FePb_3$ phase is detected in GBs. This confirmed that the interactive effect of Fe and Pb led to the stabilized grain size and then established a metastable equilibrium state. Similar results could also be obtained in the samples annealed at 500 °C and 700 °C, as shown in Fig. 1.

4.1.3. Model application of grain growth in Ni-1.5 at.% Fe-1 at.% Pb alloy

The co-segregation model (Eq. (14) with $\sigma_b = 0$) was applied to fit the experimental data, (see the solid line in Fig. 1). The parameters are shown in Table 1. From Fig. 1, this model could give a fit description of grain size evolution with annealing temperature. According to Ref. [17], σ_0 was estimated as 0.87 J m^{-2} and Γ_{20} and Γ_{30} were fitted as 1.00×10^{-5} and 2.54×10^{-5}, respectively (Table 1). ΔG_1 and ΔG_2 were fitted as 19 and 92 kJ mol^{-1}, respectively. Obviously, Fe is a weakly segregating solute and Pb is a strongly segregating element [23]. It is evidenced that the interactive effect of Pb and Fe induced the co-segregation

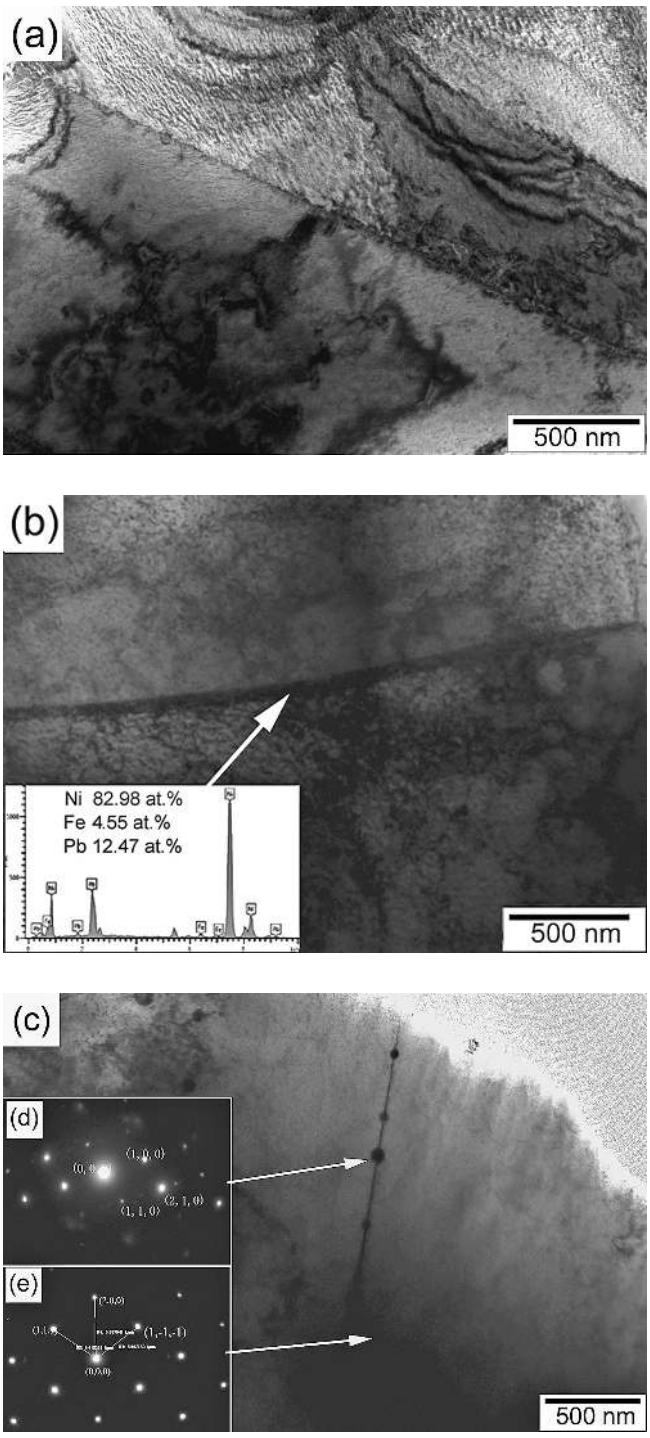

Fig. 2. Bright-field TEM images of undercooled Ni–Fe–Pb alloy at $\Delta T = 220$ K at different annealing temperatures: (a) as-solidified sample; (b) $T = 600\,^{\circ}C$; (c) $T = 800\,^{\circ}C$; (d) and (e) are the SAED patterns of the GB phase ($FePb_3$) and grain inner phase (α-Ni).

of Fe and Pb in Ni matrix (Fig. 2) and then resulted in the reduction of GB energy [18].

The case above is a metastable rather than stable equilibrium because the formation of precipitation of $FePb_3$ from saturated GBs is kinetically hindered at $T < 800\,^{\circ}C$ [7]. As for the strongly segregated system, the tendency of solute segregation to GB is very strong. It is so easy to form a saturated GB to accommodate the additional solute atoms (Fig. 2b). If the nominal impurity concentration in the alloy slightly exceeds the corresponding solubility limit, the excess impurity atoms leaving the GB should cause the nucleation of the particles of impurity-rich phase (Fig. 2c). According to the Gibbs adsorption isotherm for surfaces and GBs, with the onset of precipitation, the chemical potential may be reduced, leading to an increasing GB energy from zero and therefore providing the driving force for rapid grain growth [24]. So the grain size is larger than the calculated size at $800\,^{\circ}C$, as shown in Fig. 1. But with the further increase of annealing temperature or time, the controlled-mechanism of grain growth will transform to second phase precipitation from solute segregation, as shown in Fig. 2c [24]. Similar experimental results have been detected in NC Ni–P alloys and Al oxide. Above the solubility limit of P and yttrium, YAG and Ni_3P precipitates form and considerable grain growth occurs [25–27].

4.2. Thermal stability of NC Fe–Cr–Zr and Fe–Ni–Zr alloys

The model predictions can be compared with experimental results for NC Fe–Cr–Zr and Fe–Ni–Zr alloys prepared by ball milling [28]. Firstly, we investigated the influence of Zr and Ni solute atoms on the stability of the grain size of NC Fe–Ni–Zr produced by ball milling. Figure 3 shows the grain size vs. annealing temperature for ternary Fe–Ni–Zr alloys and binary Fe-8 at.% Ni alloy annealed at different temperatures up to $1000\,^{\circ}C$. Annealing of the as-milled nanostructured Fe-8 at.% Ni resulted in a rapid coarsening of the microstructure and the eventual coarsening to the micron scale above $600\,^{\circ}C$ [24]. Fits of Eq. (14) to the average grain sizes are shown in Fig. 3. According to Ref. [17], σ_0 was estimated as 0.73 J m^{-2} and Γ_{20}, Γ_{30}, ΔG_2 and ΔG_3 were fitted as shown in Table 1 which were close to the estimated values by Saber et al. [29]. We observed that a NC microstructure remained stable up to annealing to $700\,^{\circ}C$. It was postulated that the grain growth in Fe–Ni–Zr alloys below $700\,^{\circ}C$ was blocked by the decrease of GB energy (i.e., the driving force) induced by the co-segregation of interactive Zr and Ni [28]. Although the segregation free energy ΔG_2 is much smaller than ΔG_3, the segregation of Ni still proceeds due to the co-segregated effect.

Table 1. Physical parameters of alloys used in the calculations [15–18, 23, 29].

Parameters	Units	Fe-10Cr-*x*Zr	Fe-8Ni-*x*Zr	Ni-1.5Fe-1Pb
σ_0	J m^{-2}	0.73	0.73	0.87
Γ_{20}	mol m^{-2}	0.2×10^{-5}	0.6×10^{-5}	1.0×10^{-5}
Γ_{30}	mol m^{-2}	1.85×10^{-5}	1.85×10^{-5}	2.54×10^{-5}
ΔG_2	kJ mol^{-1}	1.6	2	19
ΔG_3	kJ mol^{-1}	92–106.2	89.7–100.1	92

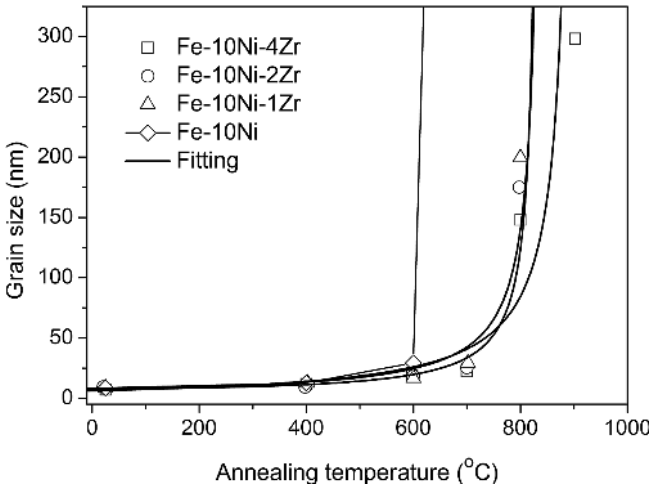

Fig. 3. Fits using Eq. (14) to the evolution of the grain size obtained in the single-phase NC solid solutions of Fe–Ni–Zr with temperature [24].

A similar prediction to the above could also be detected in the grain growth of NC Fe–Cr–Zr [28] and Fe–Zr alloys [30]. The estimated grain size versus isochronal annealing temperature for Fe-4 at.% Zr and Fe-10 at.% Cr with different amounts of Zr is plotted in Fig. 4. The addition of Cr and Zr significantly extends the stability of nano-scale grain size up to higher temperature. According to the theoretical treatment of Kirchheim et al. [7], a simpler relation was derived by differentiating Eq. (14) with respect to T as,

$$\frac{\mathrm{d}\frac{1}{D^*}}{\mathrm{d}\ln T} = \frac{(\Gamma_{20}+\Gamma_{30})\ln\left(x_2 e^{\frac{\Delta G_2}{RT}}\right) + \Gamma_{20}\ln x_3 + \Gamma_{30}\ln x_2 - H(T)}{3V_{\mathrm{m}}\Gamma_0} \tag{16}$$

$$\Gamma_0 = \Gamma_{20} + \Gamma_{30} + \frac{\left(x_2 e^{\frac{\Delta G_2}{RT}} - x_3 e^{\frac{\Delta G_3}{RT}}\right)\Gamma_{20}\Gamma_{30}}{x_2 x_3 e^{\frac{(\Delta G_2+\Delta G_3)}{RT}}} \tag{17}$$

$$H(T) = \frac{(\Gamma_{20}+\Gamma_{30})\left(\Delta G_2 x_2 e^{\frac{\Delta G_2}{RT}} + \Delta G_3 x_3 e^{\frac{\Delta G_3}{RT}}\right)}{\left(x_2 e^{\frac{\Delta G_2}{RT}} + x_3 e^{\frac{\Delta G_3}{RT}}\right)RT} \tag{18}$$

The right-hand side of Eq. (16) depends on temperature too, because the change in D^* gives rise to the change in x_i. Apparently, Eq. (16) is analogous to Eq. (13) from Liu et al. [18] and the difference between Eq. (16) and that from Liu et al. lies in whether the temperature dependence of the solute excess and segregated free energy induced by a third element are considered or not. If the effect of the third element is neglected, Eq. (16) will reduce to Liu's model (see Eq. (13) in Ref. [18]).

Figure 4 presents good agreement with Fe–Cr–Zr and Fe–Zr alloys. The detailed parameters are shown in Table 1. The physical parameters of NC Fe–Zr alloy are given in [17]. However, it is a curvilinear relationship according to Eq. (16) for data with Fe–Cr–Zr alloys. Only a linear relation with similar slopes according to data with 4 at.% Zr was given. Saber et al. [29] has shown that addition of Ni/Cr in the ternary Fe–Ni–Zr/Fe–Cr–Zr alloys affected the grain growth process. The interaction energy ($\omega^{\mathrm{Zr/Ni}}$ = –24.5 kJ mol^{-1} and $\omega^{\mathrm{Zr/Cr}}$ = –6 kJ mol^{-1} [29]) of NC Fe–Ni–Zr and Fe–Cr–Zr increases the effectiveness of thermodynamic stabilization. Combining the experimental evidence and model calculation of Ni–Fe–Pb, Fe–Ni–Zr and Fe–Cr–Zr alloys, it can further provide evidence that σ_b reduces to zero when grain growth is suppressed with saturated GBs and the interactive effect between solutes could promote the co-segregation and strengthen the thermal stability.

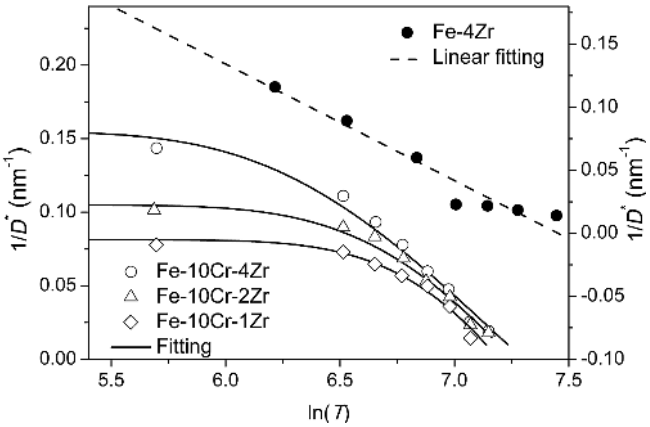

Fig. 4. Relation according to Eq. (16) for experimental data of NC Fe–Cr–Zr [28] and NC Fe–Zr [30].

5. Conclusions

The grain growth and thermodynamic stability induced by solute co-segregation in ternary alloys were presented. The main conclusions are as follows.

1. Using molten glass purification combined with cycle superheating methods and isothermal annealings, growth behavior of the single-phase supersaturated grains prepared in Ni–Fe–Pb alloy melt was analyzed.
2. Combining the multicomponent Gibbs adsorption equation and Guttmann's grain boundary segregation model, an empirical relation for isothermal grain growth was derived. By application of the model to the grain growth in Ni–Fe–Pb, Fe–Cr–Zr and Fe–Ni–Zr alloys, it was predicted that driving grain boundary energy to zero is possible in alloys due to co-segregation induced by the interactive effect between solutes Fe/Pb, Zr/Ni and Zr/Cr.
3. A non-linear relationship between 1/$D^*$and ln(T) rather than a simple linear relation was predicted due to the interactive effect.

The work was supported by the Fundamental Research Funds for the Central Universities (2015QNA27).

References

[1] T. Chookajorn, H.A. Murdoch, C.A. Schuh: Science 337 (2012) 951. PMid:22923577; DOI:10.1126/science.1224737
[2] Y.Q. Wang, Y. Guo, Z.M. Wang, Y.L. Wu: Sci. Eng. Comp. Mater. 21 (2014) 471. DOI:10.1515/secm-2013-0051

[3] J.W. Cahn: Acta Metall. 10 (1962) 789. DOI:10.1016/0001-6160(62)90092-5
[4] J.E. Burke, D. Turnbull: Prog. Met. Phys. 3 (1952) 220. DOI:10.1016/0502-8205(52)90009-9
[5] J. Weissmüller: Nanostructured Mater. 3 (1993) 261. DOI:10.1016/0965-9773(93)90088-S
[6] C.E. Krill, H. Ehrhardt, R. Birringer: Z. Metallkd. 96 (2005) 1134. DOI:10.3139/146.110931
[7] R. Kirchheim: Acta Mater. 50 (2002) 413. DOI:10.1016/S1359-6454(01)00338-X
[8] J.R. Trelewicz, C.A. Schuh: Phys. Rev. B 79 (2009) 094112. DOI:10.1103/PhysRevB.79.094112
[9] M. Guttmann: Surf. Sci. 53 (1975) 213. DOI:10.1016/0039-6028(75)90125-9
[10] T.D. Xu, B.Y. Cheng: Prog. Mater. Sci. 49 (2004) 109. DOI:10.1016/S0079-6425(03)00019-7
[11] D. Roy, B.V. Mahesh, M.A. Atwater, T.E. Chan, R.O. Scattergood, C.C. Koch: Mater. Sci. Eng. A 598 (2014) 217. DOI:10.1016/j.msea.2013.11.075
[12] M. Saber, H. Kotan, C.C. Koch, R.O. Scattergood: Mater. Sci. Eng. A 556 (2012) 664. DOI:10.1016/j.msea.2012.07.045
[13] H. Kotan, K.A. Darling, M. Saber, C.C. Koch, R.O. Scattergood: J. Alloys Compd. 551 (2013) 621. DOI:10.1016/j.jallcom.2012.10.179
[14] S. Dey, C.H. Chang, M. Gong, F. Liu, R.H.R. Castro: J. Mater. Res. 30 (2015) 2991. DOI:10.1557/jmr.2015.269
[15] Z. Chen, Y.Y. Tang, Q. Tao, Q. Chen, T. Liang: J. Alloys Compd. 662 (2016) 628. DOI:10.1016/j.jallcom.2015.11.202
[16] J.W. Gibbs: Trans. Conn. Acad. III 108 (1876); J.W. Gibbs: Trans. Conn. Acad. III 343 (1878); J.W. Gibbs: The Collected Works of J.W. Gibbs vol. 1, H.A. Bumstead (Ed.), Longmans, Green and Co, New York (1928) 55–354.
[17] Z. Chen, F. Liu, X.Q. Yang, C.J. Shen: Acta Mater. 60 (2012) 4833. DOI:10.1016/j.actamat.2012.05.029
[18] F. Liu, R. Kirchheim: J. Cryst. Growth. 264 (2004) 385. DOI:10.1016/j.jcrysgro.2003.12.021
[19] F. Liu, G.C. Yang: Int. Mater. Rev. 51 (2006) 145. DOI:10.1179/174328006X102484
[20] R. Willnecker, D.M. Herlach, B. Feuerbacher: Phys. Rev. Lett. 62 (1989) 2707. PMid:10040067; DOI:10.1103/PhysRevLett.62.2707
[21] K. Eckler, A.F. Norman, F. Gärtner, A.L. Greer, D.M. Herlach: J. Cryst. Growth 173 (1997) 528. DOI:10.1016/S0022-0248(96)01066-4
[22] Z. Chen, F. Liu, X. Yang, C.J. Shen, Y. Fan: J. Alloys Compd. 509 (2011) 7109. DOI:10.1016/j.jallcom.2011.04.014
[23] E.C. Brandes: Smithells Metals Reference Book,. E.A. Brandes, G.B. Brook (Eds.), 6th Ed., Butterworth, London (1983) 14.7–14.11.
[24] Z. Chen, F. Liu, X.Q. Yang, C.J. Shen, Y.M. Zhao: J. Alloys Compd. 608 (2014) 338. DOI:10.1016/j.jallcom.2014.04.137
[25] T. Hentschel, D. Isheim, R. Kirchheim, F. Müller, H. Kreye: Acta Mater. 48 (2000) 933. DOI:10.1016/S1359-6454(99)00371-7
[26] S.C. Mehta, D.A. Smith, U. Erb: Mater. Sci. Eng. A 204 (1995) 227. DOI:10.1016/0921-5093(95)09966-2
[27] M.A. Gülgün, R. Voitovych, I. McLaren, M. Rühle: Interface Sci. 40 (2002) 99. DOI:10.1023/A:1015268232315
[28] C.C. Koch, R.O. Scattergood, H. Kotan, M. Saber: Mater. Sci. Forum 753 (2013) 341. DOI:10.4028/www.scientific.net/MSF.753.341
[29] M. Saber, H. Kotan, C.C. Koch, R.O. Scattergood: J. App. Phys. 114 (2013) 103510. DOI:10.1063/1.4821040
[30] K.A. Darling, R.N. Chan, P.Z. Wong, J.E. Semones, R.O. Scattergood, C.C. Koch: Scr. Mater. 59 (2008) 530. DOI:10.1016/j.scriptamat.2008.04.045

(Received October 17, 2016; accepted February 9, 2017; online since April 12, 2017)

Correspondence address

Associate Professor Xiaoqin Yang
School of Chemical Engineering and Technology
China University of Mining and Technology
Xuzhou
Jiangsu 221008
P. R. China
Tel.: +86-0516-83897715
Fax: +86-0516-83591870
E-mail: xiaoqinyang@sina.com
chenzheng1218@163.com

Bibliography
DOI 10.3139/146.111496
Int. J. Mater. Res. (formerly Z. Metallkd.)
108 (2017) 6; page 435–440

ISSN 1862-5282